2020-02-15

What determines the downstream evolution of turbidity currents

Heerema, C

10.1016/j.epsl.2019.116023
Earth and Planetary Science Letters
Elsevier

Accepted version: 07/12/2019

Title: What determines the downstream evolution of turbidity currents?

Authors

Catharina J. Heerema*[1], Peter J. Talling[1], Matthieu J. Cartigny[1], Charles K. Paull[2], Lewis Bailey[3,4], Stephen M. Simmons[5], Daniel R. Parsons[5], Michael A. Clare[4], Roberto Gwiazda[2], Eve Lundsten[2], Krystle Anderson[2], Katherine L. Maier[2,6,7], Jingping P. Xu[8,9], Esther J. Sumner[3], Kurt Rosenberger[6], Jenny Gales[10], Mary McGann[6], Lionel Carter[11], Ed Pope[1], and Monterey Coordinated Canyon Experiment (CCE) Team.

Affiliations

[1] Departments of Geography and Earth Sciences, Durham University, Durham, DH1 3LE, U.K.

[2] Monterey Bay Aquarium Research Institute, Moss Landing, California 95039, USA.

[3]Ocean and Earth Science, University of Southampton, European Way, Southampton, SO14 3ZH, U.K.

[4] National Oceanography Centre, University of Southampton Waterfront Campus, European Way, Southampton SO14 3ZH, U.K.

[5] Energy and Environment Institute, University of Hull, Cottingham Road, Hull, HU6 7RX, UK.

[6] Pacific Coastal and Marine Science Center, U.S. G.S, Santa Cruz, CA 95060, U.S.A.

[7]National Institute of Water and Atmospheric Research, Wellington, New Zealand.

[8] Southern University of Science and Technology of China, Shenzhen, 518055, China.

[9] Qingdao National Laboratory for Marine Science and Technology, Qingdao, 266061, China.

[10.] University of Plymouth, Drake Circus, Plymouth, PL4 8AA, UK.

[11]. Antarctic Research Centre, Victoria University of Wellington, Wellington, New Zealand.

*Corresponding author: Catharina Heerema (email: catharina.j.heerema@durham.ac.uk).

Abstract:

Seabed sediment flows called turbidity currents form some of the largest sediment accumulations, deepest canyons and longest channel systems on Earth. Only rivers transport comparable sediment volumes over such large areas; but there are far fewer measurements from turbidity currents, ensuring they are much more poorly understood. Turbidity currents differ fundamentally from rivers, as turbidity currents are driven by the sediment that they suspend. Fast turbidity currents can pick up sediment, and self-accelerate (ignite); whilst slow flows deposit sediment and dissipate. Self-acceleration cannot continue indefinitely, and flows might reach a near-uniform state (autosuspension). Here we show how turbidity currents evolve using the first detailed measurements from multiple locations along their pathway, which come from Monterey Canyon offshore California. All flows initially ignite. Typically, initially-faster flows then achieve near-uniform velocities (autosuspension), whilst slower flows dissipate. Fractional increases in initial velocity favour much longer runout, and a new model explains this bifurcating behaviour. However, the only flow during less-stormy summer months is anomalous as it self-accelerated, which is perhaps due to erosion of surficial-mud layer with fine sands mid-canyon. Turbidity current evolution is therefore highly sensitive to both initial velocities and seabed character.

Keywords: Turbidity current; submarine canyon; ignition; dissipation; autosuspension; flow behaviour

1. Introduction

Seafloor sediment density flows (called turbidity currents) are the dominant global mechanism for transporting sediment from the continental shelf to the deep sea. These flows play a crucial role in global organic carbon burial and geochemical cycles (Galy et al., 2007), and supply of nutrients to deep-sea ecosystems (Canals et al., 2006). Only rivers transport sediment over comparable areas, although one turbidity current can carry more sediment than the annual flux from all the world's rivers combined (Talling et al., 2013). Powerful turbidity currents can badly damage seafloor infrastructure, including oil and gas pipelines, and telecommunication cable networks. The latter carry over 95% of global data traffic (Carter et al., 2014), forming the backbone of the internet and financial markets. Turbidity current deposits host valuable oil and gas reserves, and form thick sequences of ancient rocks that record Earth's history (Nilsen et al., 2008). The downstream evolution of velocities and runout lengths controls how sediment is dispersed, the resulting deposit character and shape, and hazards to seafloor infrastructure. It is thus important to understand how turbidity currents work, especially what controls their runout, and changes in flow velocity with distance.

Turbidity currents differ profoundly from terrestrial rivers; unlike rivers they are driven by the weight of sediment they carry, and this sediment can be entrained or deposited onto the seafloor along turbidity current pathways. Previous work suggested that exchange of sediment with the seabed may lead to positive feedbacks, such that turbidity current behaviour is inherently unstable and diverges (Fig. 1) (Bagnold, 1962; Parker, 1982). These studies proposed that flows which erode sediment become denser, and thus accelerate, causing increased erosion, and further acceleration (Fig. 1a). This process is called ignition, and it may play a pivotal role in producing powerful and long runout flows. Conversely, flows that deposit sediment may decelerate, leading

to further deposition ('dissipation'; Fig. 1b). Such positive feedbacks may produce thresholds in behaviour that depend on small differences in initial flow state. It has also been proposed that flows could achieve a near-uniform state in which erosion is balanced by sediment deposition, termed autosuspension (Fig. 1c, d) (Pantin, 1979). Here, turbulence within the flow is strong enough to keep particles in suspension, and counteracts their settling velocity (Parker, 1982). However, unlike ignition, there is no net gain of sediment from the bed, as the bed is too hard to erode (Fig. 1c), or sediment erosion balances sediment deposition during autosuspension (Fig. 1d). Flows that balance erosion and deposition will tend towards spatially uniform velocities, assuming that seabed gradient and flow width do not change markedly. Self-acceleration due to ignition is unlikely to continue indefinitely: increased sediment concentrations will eventually damp the turbulence that keeps sediment aloft (Baas et al., 2009) and shield the bed from rapid erosion, or increase frictional drag and thus reduce flow velocities. However, there is considerable debate over what happens after ignition ceases (Fig. 1a). Do the flows reach a state of autosuspension; and if so, what do autosuspending flows look like? In particular, do flows develop a dense near-bed layer that drives the event (as proposed by e.g. Winterwerp, 2006), or remain an entirely dilute and fully turbulent suspension (e.g. Cantero et al., 2012)?

Turbidity currents are notoriously difficult to monitor in action, due to their location, episodic occurrence, and ability to damage instruments in their path (Inman et al., 1976; Talling et al., 2013). Consequently, there are very few direct measurements from oceanic turbidity currents, ensuring fundamental theories on how turbidity currents work are poorly tested. In particular, ignition and autosuspension have been difficult to reproduce in laboratory experiments (Southard and Mackintosh, 1981). This may be because most laboratory experiments are relatively slow moving, compared to full-scale oceanic flows, and thus have limited ability to erode their

substrate, or fully support sediment with realistic grain sizes. Experimental flows thus tend to dissipate. Sequeiros et al. (2009, 2018) successfully produced self-accelerating turbidity currents in relatively slow moving (< 20 cm/s) laboratory experiments with low density particles, but they did not reproduce fully realistic processes of seabed erosion. However, new technologies have recently led to major advances in monitoring of active turbidity currents (Hughes Clarke, 2016). This includes acoustic Doppler current profilers (ADCPs) that measure velocity profiles to within a few meters of the seafloor (Xu, 2010). Here we use ADCP and other sensor data to observe spatial patterns of flow ignition, dissipation, and autosuspension in unprecedented detail; and to study how flows work in general.

This study analyses the most detailed (7 locations at sub-minute intervals) field measurements yet from oceanic turbidity currents, which include the fastest (up to 7.2 m/s) flows captured via moored instruments. These measurements come from the upper 52 km of Monterey Canyon, offshore California (Fig. 2a) (Paull et al., 2018). Previous direct monitoring of turbidity currents has typically involved measurements at a relatively small number (≤3) of locations along their pathway, which provides limited information on how flows behave (Khripounoff et al., 2009; Liu et al., 2012; Azpiroz-Zabala, 2017). By having measurements in seven locations along a turbidity current pathway we are able to determine how flows evolve. Here we focus on changes in the average flow front velocities between measurement locations (termed transit velocities), maximum internal velocities, as well as duration of flow velocities in each event (as measured by ADCPs).

1.1. Aims

The first aim is to document changes in turbidity current velocity and runout distance, and hence flow behaviour. What is the observed pattern of ignition, autosuspension and dissipation; and do multiple flows show a consistent pattern of behaviour? The second aim is to understand what causes these patterns of flow behaviour. In particular, we consider how two factors (initial velocity and substrate erodibility) affect flow behaviour, and how near-uniform flow (autosuspension) may follow ignition. Our third aim is to determine if broadly similar flow behaviour is seen elsewhere, although suitable field data are sparse. Our fourth aim is to compare these field observations to most widely accepted theories for ignition and autosuspension. To what extent do these new field data provide a test of past theories? Finally, we develop a new generalised model for how turbidity currents in submarine canyons floored by loose sand operate, which better explains these novel field observations.

1.2. Terminology

Turbidity current is used here as a general term for all types of submarine sediment density flow. *Dense flow* signifies sediment concentrations that are high enough to damp turbulence significantly, such that turbulence is no longer the main support mechanism, whilst *dilute flow* is fully turbulent. There is no single threshold value for sediment concentration at which turbulence is strongly damped, as this depends on multiple factors including flow velocity, sediment mineralogy and grainsize. But dilute flows typically have sediment concentrations of << 1%, whilst dense flows might often contain > 10% sediment by volume. *Diverging* behaviour denotes how small changes in initial flow velocity are linked to large changes in subsequent runout. It does not imply that flow behaviour is bimodal, and intermediate runout lengths can still occur.

2. Material and Methods

The Coordinated Canyon Experiment (CCE) monitored the upper 50 km of Monterey Canyon (California, USA) to water depths of 1850 m, for 18 months from 2015 to 2017 (Fig. 2) (Paull et al., 2018). Sand is primarily delivered to the canyon head via longshore drift, with little river input (Paull et al., 2005). The entire canyon-channel system extends for over 300 km, but flows that runout for over 60 km, to a water depth of 2,850 m, only occur every few hundred years (Stevens et al., 2014). Flows are confined, and experience a constant seafloor gradient and width in the upper part of Monterey Canyon (Fig. 3). The upper Monterey Canyon, up to 2100 m water depth, has a sinuosity of 1.9 (Paull et al., 2011). The canyon briefly narrows at a constriction between 1300 and 1400 m water depth, called the Navy Slump (Figs. 2 and 3) (Paull et al., 2011). This study uses data recorded by ADCPs along the canyon thalweg (Fig. 2), which were part of a larger instrumental array (Supplementary fig. 1) (Paull et al., 2018).

2.1. ADCP measurements

ADCPs documented velocity profiles through the turbidity currents (Fig. 3; Supplementary Fig. 1), although they are typically unable to make measurements within a few meters of the bed. The shallowest five mooring stations (MS1 to 5), and deepest mooring station (MS7), had downward-looking 300 kHz ADCPs located approximately 65 m above the bed seafloor (Paull et al., 2018). ADCPs on these moorings recorded velocity at 30 second intervals. A Seafloor Instrument Node (SIN) was located between MS5 and MS7, which contained three separate upward-looking ADCPs recording at 10 second intervals, using acoustic sources with three different frequencies (300, 600, 1200 kHz). No reliable ADCP measurements of current velocity are available from the shallowest mooring (MS1) for some flows, as this mooring broke loose on January 15, 2016 (Paull et al., 2018).

2.2. Maximum flow velocity measured by ADCPs

Determining the maximum reliable velocity measured by the ADCP is not straightforward. The arrival of an event is accompanied by mooring tilt and high near-bed sediment concentrations, influencing the ability of ADCPs to accurately record velocities (Paull et al., 2018). Side-lobe interference may compromise some ADCP measurements within 1-3 m of the seabed (Teledyne RD Instruments, 2011), although this depends on the relative strength of backscatter from side-lobe areas and sediment in the flow. We thus adopted a consistent procedure for calculating maximum ADCP-measured velocities, which excludes the 20 highest values during an event. The overall trend of internal velocities remains the same, and therefore our ADCP data processing does not change this paper's main conclusions.

2.3. Transit velocities and runout distance

Flow arrival times at the 6 ADCP moorings and SIN were used to measure transit velocities, which are average front velocities across distances between 0.5 km and 15 km (Fig. 3a). Arrival times are based on 30 second (or 10 second for SIN) recording interval of the ADCPs, corrected for clock drift. Distances between sensors were measured along the canyon thalweg, based on a 15 m bathymetric grid. It is assumed that flows principally followed the thalweg (Fig. 2a).

2.4. Duration of powerful flow measured by ADCPs

As frontal or maximum velocities only tell part of how flow is evolving, and changes in velocity structure, the duration of a fast-moving flow is also quantified and presented (Table, 1;

Supplementary fig. 4). This duration, determined for three different velocity thresholds, provides an additional indication of how flows may lengthen or stretch over time.

2.5. Canyon topography

Seafloor gradient is determined along a midline through the canyon thalweg (Fig. 3b), using an average of 10 grid-cells, each of which has a length of 15 m. Canyon width is defined using the area of active bedforms (Paull et al., 2018), and measured every 200 m down the canyon. The canyon floor is delimited by steep canyon walls with slopes of ~10 to 45°.

2.6. Grain sizes

Sediment traps were mounted at 10 meters above the seafloor on moorings (Supplementary fig. 1). They were tilted and brought closer to the bed by the initial powerful stages of some flows. Grain sizes in sediment traps from the upper canyon (MS1, MS2, and MS3) were used for most events. For the September 1st event, MS3 and MS4 are used, as the event ignited farther down in the canyon. Laser particle grain size measurements were taken every 1-5 cm from traps. Discs released automatically into the traps at 8-day intervals provided time markers. Supplementary fig. 5 shows grain size distribution for the flow events, including mean grain sizes used for Fig. 6.

3. Results

The entire sensor array in Monterey Canyon recorded 15 flows (Paull et al., 2018). Here we consider only the 13 flows measured using the moored ADCP array (Fig. 2b; Supplementary figs. 1 and 2), as we rely on ADCP measurements. Twelve of these 13 ADCP-measured flows started in the upper canyon at water depths of < 300 m. Flows were measured first by ADCPs at Mooring Station (MS) 1, located 6.7 km from the canyon head (Figs. 2a and 3a). Many flows

then rapidly dissipated, including six flows that died out entirely before MS2, which is 9 km downstream of MS1 (Fig. 3a). Of the seven flows measured at multiple moorings, three flows terminated within the sensor array. One event occurred only in the mid-canyon, between MS4 and MS5. Three further flows swept through the entire sensor array, running out for over 50 km from the canyon head, although they had very different velocities and durations at the final sensor site (Fig. 4). Most (12 of 13) flows were initiated during the winter months (Fig. 2b), during which time storm waves are most pronounced and are thought to be important for flow initiation (Paull et al., 2018). Only one event occurred in the summer months. This event on September 1st 2016 did not coincide with large wave heights, a river flood, or earthquake; suggesting another, as yet poorly understood, trigger (Paull et al., 2018).

Transit velocities are available for the seven flows that reached multiple moorings (Fig. 3a). The transit velocities between the first two moorings (MS1 and MS2) have broadly similar values of between 4 and 6 m/s. The runout length of these flows varied greatly, with large increases in runout length correlating with only slightly faster initial frontal velocity (Fig. 3a). However, one event recorded during the CCE experiment showed a different trend, and it was the only event occurring outside the winter months, on September 1st (Fig. 1b). This event started with an initial comparatively low frontal velocity between MS1 and MS2 of ~4 m/s, identical to the initial frontal velocity of the November 24th event (Fig. 1c) (Paull et al., 2018). However, the November 24th event failed to reach MS3; whilst the September 1st event accelerated between MS3 and MS5, and reached the end of the instrument array (Fig. 3a).

The maximum ADCP velocities measured within flows occurred within the first 10 minutes of the flow front arrival. These internal velocities show a broadly similar pattern to the transit

velocities (Fig. 3a). Flows with slower maximum ADCP-measured velocities at the first mooring tended to die out abruptly in the upper canyon, whilst events with faster ADCP-measured velocities ran out for much longer distances (Fig. 3a). Note that ADCP measurements define six shorter runout events that are only recorded at one mooring, and thus lack transit velocity data.

Flow behaviour is only partly captured by transit and maximum ADCP measured velocities. For example, modest increases in transit velocity are often associated with more prolonged periods of powerful flow (Fig. 4, Table 1). As a powerful flow is more efficient in entraining substrate, the duration of powerful flow is important for ignition or autosuspension. Flows tend to stretch, as the frontal part of the flow runs ahead from the slower moving body and tail (Fig. 4) (Azpiroz-Zabala, 2017). Overall, long run-out events occurring in winter tended to significantly stretch, such that they extended for almost the entire length of the instrument array. Shorter winter events, based on data from the shorter winter event on November 24th, are initially ~10 km in length as the event arrives at MS2, but die out in the upper-canyon. The long runout summer event was initially weak, but became much more prolonged and faster mid-canyon, as well as increasing its transit velocity; before dissipating rapidly between MS5 and MS7 (Fig. 4). Most flows started with a flow front thickness <10m. The long run-out events in winter developed thicknesses >30 m (Fig. 4) (Paull et al., 2018).

4. Discussion

4.1. Is there a consistent pattern of behaviour for turbidity currents?

Eleven of the twelve flows show a broadly consistent pattern of runout behaviour, which can be based on the initial transit velocity between the first two moorings, and the maximum ADCP-

measured velocities at the first mooring (Fig. 3a). Flows with the fastest initial velocities tend to run out further. However, small changes in initial transit velocities, or maximum ADCP-measured velocities, lead to much larger changes in runout distance and subsequent flow velocity. Runout distances are thus highly sensitive to initial velocities, leading to diverging flow behaviour (Fig. 3a). All flows initially accelerate, and the initially fastest flows have near-uniform transit velocities for several tens of kilometres and can stretch up to 35 km in length (4). Flows with only fractionally slower (~0.5 m/s) initial transit velocities, or maximum ADCP-measured velocities, die out mid-canyon. The six slowest moving flows at MS1 terminate rapidly before reaching MS2 (Fig. 3a). These flows that die out in the upper or mid-canyon are initially powerful, and can sometimes carry heavy (800 kg) objects, or move moorings down-canyon, at velocities of ≥4 m/s, but their power does not persist for several kilometres. Only the fastest flows at the first mooring maintain their velocity for longer distances, and lengthen significantly. The single exception to this general pattern of behaviour (Figs. 2c and 3) occurred on September 1st 2016. This flow's transit velocity and maximum ADCP-measured velocity increased in the mid-canyon (Fig. 3a), and the duration of powerful flow lengthened markedly (Fig. 4).

These field data thus provide new insights into where and how flows ignite, dissipate or autosuspend. A notable observation is that the four most powerful flows at MS1 have near-uniform transit velocities for ~20-35 km, from MS1 to MS3; and near-uniform maximum internal (ADCP-measured) velocities from MS1 to MS2 (Fig. 3a). This suggests that an initial phase of acceleration (ignition) is followed by near-uniform flow velocities (autosuspension), at least near the flow front. Transit velocities are averages over substantial distances, and internal (ADCP-measured) velocities come from a few specific locations. Thus, it is possible that flow velocities

show greater localized variability than depicted in Fig. 3a. However, available field data indicate near-uniform transit velocities (autosuspension) over substantial distances.

4.2. What factors control turbidity current behaviour?

We now seek to understand what controls these patterns of flow behaviour. Twelve flows accelerated rapidly from rest within the upper 6.7 km of the canyon, reaching velocities of at least 3 to 6 m/s at MS1 (Fig. 2). These turbidity currents were most likely generated by seabed failure, typically during storm events, as sediment plumes from rivers are weak or absent (Paull et al., 2018). An initial phase of acceleration will partly result from gravitational acceleration of the failed mass, but it may also indicate that flows eroded the seabed and self-accelerated (ignited). However, the relative importance of simple gravitational acceleration of an initial failure, and ignitive self-acceleration via subsequent seabed erosion, is uncertain due to a lack of repeat bathymetric surveys with high enough frequency upstream of MS1.

Beyond MS1, small (< 0.5-1 m/s) increases in initial transit or maximum ADCP-measured velocities are associated with profound differences in subsequent flow behaviour (Figs. 2c and 3). We thus infer that initial velocities in the upper canyon determine later flow behaviour. Flows with only fractionally higher initial transit velocities, or maximum internal ADCP-measured velocities, tend to run out for much greater distances (Fig. 3a; Table 1). This strongly diverging flow behaviour is not due to changes in seafloor gradient or canyon width, as canyon axial channel width (~200 m) and gradient (~ 2°) are relatively uniform from MS1 to MS3 (Fig. 2d, e), and all of these flows experienced similar changes in canyon slope and width. However, the axial channel widens significantly beyond MS3 (from ~200 to ~600 m), which may explain why most flows consistently decelerate beyond MS3 and MS4 (Fig. 3).

The September 1st event is anomalous, as it was initially slow moving but its transit velocity then increased mid-canyon (Fig. 3a), and the duration of powerful flow velocities increased (Fig. 4; Table 1). This acceleration is not related to steepening or narrowing of the canyon, and cannot be explained by a 'tail wind' from internal tides (Supplementary Fig. 3). This flow was also the only event to occur in summer (Fig. 2b). One hypothesis is that self-acceleration of the September 1st event resulted from entrainment of a surficial-mud layer, deposited during less-stormy summer months. Surficial-mud layers that are 1-12 cm thick occur in the nearby La Jolla Canyon (Paull et al., 2013), whilst mud layers in cores from MS7 in Monterey Canyon are 1-3 cm thick, with modal grain sizes of ~50-80 μm (Fig. 8 of Maier et al., 2019). However, it is not clear whether surficial-mud layers are better developed during summer months, as information from repeat coring during different seasons is lacking. Moreover, strong (50-80 cm/s) internal tides in Monterey Canyon rework canyon floor mud throughout the year (Maier et al., 2019). An alternative hypothesis for mid-canyon ignition of the September 1st event is triggering of a local substrate failure, forming a knickpoint. Such knickpoints are observed in several places on the canyon floor, and they have been termed 'master head scarps' in past work (Paull et al., 2010). However, we also lack suitably detailed time-lapse seabed surveys from the mid-canyon to determine whether a local knickpoint failure occurred.

4.3. Do submarine flows in other locations show similar behaviour?

Having determined that there is a consistent pattern of flow behaviour in Monterey Canyon, albeit with one exception, we now seek to understand if similar behaviour occurs elsewhere, and is thus of more general importance. There are few other locations worldwide where the transit or

internal velocities of oceanic turbidity currents have been measured at more than 4 locations along the flow pathway. Indeed, we are aware of only 3 such datasets (Fig. 5).

One of these field datasets comes from cable breaks along Gaoping Canyon, offshore Taiwan, which (unlike Monterey Canyon) is fed by a major river mouth (Fig. 5b) (Gavey et al., 2017). Seabed gradients along Gaoping Canyon (0.3°-1.0°; Gavey et al., 2017) are somewhat lower than Monterey Canyon (1.6°- 2.3°; Paull et al., 2011) (Fig 5). Transit velocities in Gaoping Canyon are nearly constant for ~100 km, suggesting that the turbidity currents reach a near-uniform equilibrium state. This pattern of uniform flow front velocities (autosuspension) is thus not specific to Monterey Canyon, and it may persist over even longer distances.

A second data set comes from a turbidity current that broke submarine cables offshore from the Grand Banks, Newfoundland, in 1929 (Heezen and Ewing, 1952; Piper et al., 1988). The turbidity current resulted from extensive but thin (average 5 m) failures on the continental slope, with ~ 185 km^3 of sediment deposited on the Sohm Abyssal Plain (Piper and Aksu, 1987; Piper et al., 1988). These failures progressively entrained seawater and evolved into debris flows, and then turbidity currents (Piper et al., 1999). Flow was confined initially within multiple valleys for the first ~500 km of the pathway (Hughes Clarke et al., 1990), where it reached a transit velocity of 19 m/s on a gradient of ~0.5° (Hughes Clarke et al., 1988). This initial phase of the flow eroded the seabed, and may have ignited; although this is not demonstrated by flow velocities from cable breaks. Transit velocities then decreased to 6.2 m/s on gradients of ~0.15 to 0.05°, as flow became poorly confined, and spread to become several hundred kilometres wide (Fig. 5c; Heezen and Ewing, 1952; Hughes Clarke, 1988; Hughes Clarke, 1990; Piper and Hundert, 2002).

Its transit velocity continuously decreased with distance during these later stages, showing how reduction in confinement can control flow behaviour, leading to dissipation.

4.4. Comparison of field data to previous theory of autosuspension and ignition

We now compare our new field observations to previous influential theory that predicts when a submarine turbidity current will autosuspend or ignite (Bagnold, 1962; Pantin, 1979; Parker, 1982; Parker et al., 1986). It is important to understand whether these unusually detailed field observations can provide a robust test of such theories.

4.4.1. Initial energy-balance theory

Initial work (Bagnold, 1962; Pantin, 1979; Parker, 1982) formulated a theory for whether turbidity currents autosuspend or ignite that is based on energy losses and gains by the flow. It was assumed that movement of sediment down-slope results in loss of potential energy, whilst energy is expended by processes that keep sediment grains aloft. When energy gains equal or exceed energy losses, the flow can carry all of the sediment it suspends. Then, if the flow can also erode loose sediment from the bed, it ignites (Fig. 1). However, if no erodible material is available, the flow autosuspends. Alternatively, if energy losses exceed energy gains, then some of the suspended sediment will settle out, and the flow will eventually dissipate.

Equation 1 and figure 6 result from this initial energy-balance theory (Bagnold, 1962; Pantin, 1979; Parker, 1982), as previously depicted by Sequeiros et al. (2009). Figure 6 predicts the threshold frontal velocity (u_h) for ignition, as a function of sediment settling velocity (w_s) and seafloor gradient (β). The threshold constant for ignition to occur (ε), varies between different

authors. Bagnold (1962) and Parker (1982) assume that potential energy gain must at least equal or exceed energy losses ($\varepsilon \leq 1$). In contrast, Pantin (1979) assumes that only a small fraction ($\varepsilon \leq 0.01$) of potential energy gain will be available to keep sediment aloft, with most potential energy being dissipated in other ways.

$$Equation\ (1) \qquad \frac{w_s cos\beta}{u_h sin\beta} \leq \varepsilon \begin{cases} \varepsilon = 0.01 & (Pantin, 1979) \\ \varepsilon = 1 & (Parker, 1982) \\ \varepsilon = cos\beta & (Bagnold, 1962) \end{cases}$$

As we use the flow front velocity (u_h), we only consider whether ignition or autosuspension occurs near the flow front. As noted by past authors (e.g. Bagnold, 1962; Pantin, 1979; Parker, 1982; Sequeiros et al., 2009), Equation 1 is a necessary condition for ignition, but it is not a sufficient condition for ignition; indeed it is rather conservative (Parker et al., 1986). Suitable sediment must also be available for erosion and incorporation into the flow. This might not be the case, for example, if the flow was moving over hard bedrock.

Measurements from Monterey Canyon can be combined with Equation 1 to compare observed and predicted flow velocities associated with ignition (Fig. 6). We use a seabed gradient of 2° (Fig. 1e) (Paull et al., 2018), and sediment traps on moorings for grainsize distributions for three separate turbidity currents. The sediment trap closest to the location of ignition in that flow is used (Fig. 1c), together with the coarsest subsample from each flow deposit in that trap. These traps were initially suspended 10 m above the bed, but they were sometimes dragged closer to the bed during the first few minutes of flow (Paull et al., 2018). The method of Ferguson and Church (2004) is used to estimate settling velocities for individual grains, which assumes that flow is dilute. Settling velocities could become hindered at higher sediment concentrations.

Figure 6 shows transit (average frontal) velocities needed for ignition for the grain sizes captured by traps in the Monterey Canyon flows, for different values of ε that have been proposed previously. There is reasonable agreement between our field observations with the approach of both Parker (1982), and Bagnold (1962). Where flows ignited in Monterey Canyon, grain sizes observed in sediment traps mainly lie within the field of ignition (Fig. 6). There is poorer agreement with Pantin (1979), suggesting that potential energy losses do not need to be 100 times greater than energy losses to keep sediment aloft, and thus for ignition to occur.

4.4.2. Subsequent more complex turbulence energy-balance theory

The simple energy-balance approach summarized by equation 1 (Bagnold, 1962; Pantin, 1979; Parker, 1982) sets out a necessary condition for autosuspension or ignition. However, flows that fulfil equation 1 need not ignite, as other conditions are also important. For example, sediment exchange with the seabed will strongly influence flow density and thus velocity (Parker et al., 1986; Traer et al., 2012), whilst entrainment of surrounding water will cause momentum to be lost (Parker et al., 1986).

Parker et al. (1986) therefore subsequently developed a more advanced and complete theory. This theory initially comprised three layer-averaged equations based on budgets of fluid (water) mass, sediment mass and momentum within the flow (Parker et al., 1986). A fourth layer-averaged equation was then based on budgets of turbulent kinetic energy within the flow, including turbulence production at the upper and lower flow boundary, dissipation of turbulence due to viscosity, and work done by turbulence against vertical density gradients (Parker et al., 1986).

This approach led to a more complex criterion for ignition (equation 16 of Parker et al. (1986)). This criterion involves layer-averaged sediment concentration, flow velocity and thickness, sediment settling velocity, bed shear velocity, and rates of sediment and water entrainment (Parker et al., 1986). This more advanced but complex criterion for ignition implicitly assumes that sediment is mainly supported by fluid turbulence. It would not apply to denser sediment flows in which turbulence is strongly damped, and where other processes become important for sediment support, such as support via grain-to-grain collisions, or excess pore pressure.

4.5. Why past autosuspension and ignition theory is difficult to test

Although unprecedented in their detail, our field observations from Monterey Canyon provide a rather weak test of the initial simpler energy-balance theory (Bagnold, 1962; Pantin, 1979; Parker, 1982), and they are unable to test the more complex turbulent energy-balance (Parker et al., 1986) theory, for three key reasons.

First, both types of theory involve a single sediment settling velocity, and thus require that a representative grain size is chosen. However, turbidity currents in Monterey Canyon contain a wide range of grain sizes (Fig. 6), as is often the case for turbidity currents elsewhere. Thus, there is an issue of which representative grain size to choose from this wide distribution (Fig. 6). There are also major issues related to measurement of grain size in the field via sediment traps, as traps only sample grain size at a single height, and traps may be less effective at capturing finer grains than coarser grains.

Second, in the case of theory based on turbulent kinetic energy budgets (Parker et al., 1986), we lack sufficiently precise measurements of key parameters needed by this theory, most notably layer-averaged sediment concentrations, but also rates of sediment and water entrainment.

Finally, and most importantly, some key assumption that underpin past theories may not hold. For example, Parker's later theory based on turbulent kinetic energy budgets assumes that flow is dilute, such that turbulence is always the main support mechanism (Parker et al., 1986). Field evidence suggests that some turbidity currents in Monterey Canyon are driven by dense near-bed layers with high (> 10% by volume) sediment concentrations (Fig. 6) (Paull et al., 2018). These dense layers are needed to explain the fast (≥4 m/s) movement of very heavy (up to 800 kg) objects for several kilometres (Paull et al., 2018). It is unlikely that entirely dilute flows could carry such heavy objects, at high velocities, for such distances; the heavy objects are instead entombed in a dense near-bed layer (Paull et al., 2018). Turbulence is damped strongly in such dense near-bed layers, and settling will be hindered (Winterwerp, 2006). Other sediment support mechanisms become important, such as grain collisions or excess pore pressures that partly carry the sediment load. The more advanced ignition theory (Parker et al., 1986) would thus be unable to capture the behaviour of flows in Monterey Canyon with dense near-bed layers.

4.6. New travelling wave model

We now outline a new conceptual model for how initially fast moving turbidity currents operate in confined settings, underlain by loose sand, based on our field observations. Following Paull et al. (2018), this model includes dense near-bed layers that drive the flow, in which turbulence is not the main support mechanism. The model thus better fits detailed field observations from

Monterey Canyon. A new model is needed because past theory for ignition and autosuspension (Parker et al., 1986) was not formulated to include dense near-bed layers. The new model differs from past work (e.g. Paull et al., 2018), as it explains how flows that initially ignite may then autosuspend, as they reach a uniform transit velocity.

We propose that during initial ignition, and the following near-equilibrium (autosuspension) phase, a fast and dense near-bed layer exists at the flow front, which drives the overall event, similar to Fig. 7 (Winterwerp, 2006). This dense near-bed layer near the flow front maintains an approximately uniform frontal velocity, as erosion of the bed near its front, is balanced by deposition at its rear (Fig. 7). Thus, although the dense layer is locally either erosive or depositional at a single location, erosion and deposition are balanced over the whole of the layer, such that the dense layer velocity is near-uniform. This leads to autosuspension (Fig. 7). We envisage that sediment concentrations in the dense layer (10-30%) are those attributed by Winterwerp et al. (1992) to hyperconcentrated flow, which is capable of forming the crescentic shaped bedforms seen along the floor of Monterey Canyon (Winterwerp et al., 1992; Paull et al., 2018). It has been suggested that liquefied flows of sand could only travel for short distances (Lowe, 1976) on steep slopes (>3°) due to rapid dissipation of excess pore fluid pressures and basal sedimentation. However, addition of small fractions of cohesive mud, as seen in Monterey Canyon (Maier et al., 2019), increase the time taken for excess pore pressure to dissipate by orders of magnitude and hinders settling (Iverson et al., 2010), thus greatly increasing runout of partly-liquefied flow. Sediment from the dense layer is shed backwards into a dilute and fully turbulent sediment cloud. This trailing cloud increases in length (stretches) as the dense flow front runs ahead of the trailing body (Figs. 3 and 6) (Azpiroz-Zabala et al., 2017).

We term this new model the 'travelling wave model', and it is broadly comparable to behaviour seen in laboratory experiments involving dense, dry granular avalanches (Supplementary fig. 6) (Pouliquen and Forterre, 2002; Mangeney et al., 2007). A key feature of these experiments is that the dry avalanches that are fast enough can erode their underlying substrate, in their case loose sand. These dry granular avalanche experiments show two types of behaviour (Pouliquen and Forterre, 2002; Mangeney et al., 2007). Slower moving avalanches dissipate, as they fail to erode and entrain their substrate. However, sufficiently fast moving dry granular avalanches erode, and form a travelling wave with near-uniform frontal transit velocities (Supplementary fig. 6) (Pouliquen and Forterre, 2002; Mangeney et al., 2007; Edwards and Gray, 2015). Erosion of sand from near the front of the travelling wave is balanced by deposition from its rear (Fig. 7). The avalanche thus contains a substantial fraction of locally eroded material. The transit velocity of this travelling wave is strongly determined by the thickness of the frontal avalanche, as in the dry granular experiments (Pouliquen and Forterre, 2002; Mangeney et al., 2007). Frontal thickness determines the down-slope driving force near the front, at least for near-uniform gradients and flow densities. The flow thickness in turn depends on the depth of eroded material, and thus on rates of frontal erosion (Pouliquen and Forterre, 2002; Mangeney et al., 2007). Turbidity currents will differ in key regards from these dry granular avalanches that occur on far steeper (> 30°) gradients. For example, erosion of water-saturated canyon floor sediment, such as via abrupt loading and liquefaction, may allow turbidity currents to erode on much lower (< 2°) gradients than dry granular avalanches. Settling velocities will be much greater in air, and turbidity currents can also comprise trailing dilute suspensions. However, we draw a first-order analogy with the ability of faster moving dry granular avalanches that exceed a threshold and erode their substrate, whilst depositing from their rear, and thus maintain dense flow with near-uniform transit velocity.

509 This new travelling wave model also needs to account for crescent shaped bedforms that are
510 abundant along the floor of Monterey Canyon (Paull et al., 2018), and many other sandy
511 submarine canyons (Symons et al., 2016), which have been linked to instabilities (termed cyclic
512 steps) in supercritical flows (Hughes Clarke, 2016). Bedforms in Monterey Canyon have
513 amplitudes of 1 to 3 m, and wavelengths of 20 to 80 m (Paull et al. 2018). As discussed in more
514 detail by Paull et al. (2018), tracking of extremely heavy (800 kg) objects showed that they
515 experienced repeated vertical oscillations of 1-3 m, as they were carried down Monterey Canyon
516 at velocities of ~4 m/s. Bedforms were thus most likely continuously present, and must have been
517 at least partly formed by the dense travelling wave. This is consistent with field observations and
518 laboratory experiments showing that cyclic steps and up-slope migrating bedforms can form
519 beneath supercritical flows with very high (20-40% volume) sediment concentrations
520 (Winterwerp et al., 1990, 1992) as well as dilute supercritical flows (Kostic and Parker, 2006;
521 Covault et al., 2017).

522 Future work is now needed to test this new travelling wave model, such as via direct
523 measurements of sediment concentration in turbidity currents, or by determining the importance
524 of locally derived or far-travelled sediment in near-bed layers.

525

526 **5. Conclusions**

527 Here we analyse the most detailed measurements yet from within seafloor turbidity currents,
528 showing how their transit and maximum measured internal velocities vary with distance.

529

530 Overall, we observed that small (< 0.5-1 m/s) increases in average transit velocities are associated
531 with large differences in subsequent runout (Fig. 8). Fractional increases in initial velocities may

lead to flows with near-uniform velocities associated with autosuspension, enabling much longer runout. Flows with only slightly lower initial velocities die out in upper or mid-canyon. Patterns of transit and internal velocities with distance thus diverge markedly (Fig. 8).

However, one flow in Monterey Canyon is an exception to this general pattern, as it self-accelerated mid-canyon (Fig. 8, dotted green line). It is also the only flow that occurred during less-stormy summer months. Erosion of a weak surficial-mud layer with underlying fine sand, is likely to also favour self-acceleration. Turbidity current behaviour may therefore be highly sensitive to both initial transit velocities and substrate character.

Our observations show that initial self-acceleration (ignition) can be followed by a phase of near-uniform transit velocities (autosuspension), at least for initially faster flow events (Fig. 8). Previous models have proposed that autosuspension may follow on from ignition, as erodible bed material runs out. But this is not the case in Monterey Canyon, as loose sand is available along the canyon floor. Instead, we propose that flows are driven by thin and dense, frontal, near-bed layers (which we call a travelling wave; Fig. 7). Faster moving travelling waves can reach an autosuspending state, as frontal erosion balances deposition from their rear, so that near-uniform frontal flow thicknesses and thus velocities are maintained. These dense travelling waves shed a slower moving dilute sediment cloud, which lengthens as the flow runs out. But this dilute cloud does not drive the flow, and changes in its sediment concentration are thus less important. This travelling wave model itself needs further testing, including via direct measurements of near-bed sediment concentrations, but it is consistent with movement of very heavy objects at high velocity near the flow front (Paull et al., 2018).

Acknowledgments

C.J. Heerema is funded by the European Union's Horizon 2020 research and innovation program under the Marie Skłodowska-Curie grant agreement No 721403 - ITN SLATE. This project received funding from the David and Lucile Packard Foundation, Natural Environment Research Council (grant NE/K011480/1), U.S. Geological Survey (USGS) Coastal and Marine Program, and Ocean University of China. We acknowledge NERC funding (NE/K011480/1, NE/M007138/1, NE/M017540/1, NE/P009190/1, and NE/P005780/1). M.A. Clare acknowledges support from NERC National Capability project Climate Linked Atlantic Sector Science (NE/R015953/1). E. Pope was supported by a Leverhulme Trust Early Career Fellowship (ECF-2018-267).

Data and materials availability

Data are available at https://doi.org/10.1594/IEDA/324529.

References

Azpiroz-Zabala, M., Cartigny, M.J.B., Talling, P.J., Parsons, D.R., Sumner, E.J., Clare, M.A., Simmons, S.M., Cooper, C., Pope, E.L., 2017. Newly recognized turbidity current structure can explain prolonged flushing of submarine canyons. Science Advances 3, e1700200. https://doi.org/10.1126/sciadv.1700200

578 Baas, J.H., Best, J.L., Peakall, J., Wang, M., 2009. A Phase Diagram for Turbulent, Transitional, and
579 Laminar Clay Suspension Flows. Journal of Sedimentary Research 79, 162–183.
580 https://doi.org/10.2110/jsr.2009.025

581 Bagnold, R.A., 1962. Auto-suspension of transported sediment; turbidity currents. Proceedings of the
582 Royal Society of London 265, 315–319. https://doi.org/10.1098/rspa.1962.0012

583 Canals, M., Puig, P., Madron, X.D. de, Heussner, S., Palanques, A., Fabres, J., 2006. Flushing submarine
584 canyons. Nature 444, 354–357. https://doi.org/10.1038/nature05271

585 Cantero, M.I., Cantelli, A., Pirmez, C., Balachandar, S., Mohrig, D., Hickson, T.A., Yeh, T., Naruse, H.,
586 Parker, G., 2012. Emplacement of massive turbidites linked to extinction of turbulence in
587 turbidity currents. Nature Geoscience 5, 42–45. https://doi.org/10.1038/ngeo1320

588 Carter, L., Gavey, R., Talling, P., Liu, J., 2014. Insights into Submarine Geohazards from Breaks in Subsea
589 Telecommunication Cables. Oceanography 27, 58–67. https://doi.org/10.5670/oceanog.2014.40

590 Edwards, A.N., Gray, J.M.N.T., 2015. Erosion–deposition waves in shallow granular free-surface flows.
591 Journal of Fluid Mechanics 762, 35–67. https://doi.org/10.1017/jfm.2014.643

592 Ferguson, R.I., Church, M., 2004. A Simple Universal Equation for Grain Settling Velocity. Journal of
593 Sedimentary Research 74, 933–937. https://doi.org/10.1306/051204740933

594 Galy, V., France-Lanord, C., Beyssac, O., Faure, P., Kudrass, H., Palhol, F., 2007. Efficient organic carbon
595 burial in the Bengal fan sustained by the Himalayan erosional system. Nature 450, 407–410.
596 https://doi.org/10.1038/nature06273

597 Gavey, R., Carter, L., Liu, J.T., Talling, P.J., Hsu, R., Pope, E., Evans, G., 2017. Frequent sediment density
598 flows during 2006 to 2015, triggered by competing seismic and weather events: Observations

599 from subsea cable breaks off southern Taiwan. Marine Geology 384, 147–158.
600 https://doi.org/10.1016/j.margeo.2016.06.001

601 Gladstone, C., Sparks, R.S.J., 2002. The Significance of Grain-Size Breaks in Turbidites and Pyroclastic
602 Density Current Deposits. Journal of Sedimentary Research 72, 182–191.
603 https://doi.org/10.1306/041801720182

604 Heezen, B.C., Ewing, W.M., 1952. Turbidity currents and submarine slumps, and the 1929 Grand Banks
605 [Newfoundland] earthquake. American Journal of Science 250, 849–873.
606 https://doi.org/10.2475/ajs.250.12.849

607 Hughes Clarke, J.E., 1988. The geological record of the 1929 Grand Banks earthquake and its relevance to
608 deep-sea clastic sediment. Dalhousie University, Nova Scotia, Canada. 171 pp.

609 Hughes Clarke, J.E., 2016. First wide-angle view of channelized turbidity currents links migrating cyclic
610 steps to flow characteristics. Nature Communications 7, 11896.
611 https://doi.org/10.1038/ncomms11896

612 Hughes Clarke, J.E., Shor, A.N., Piper, D.J.W., Mayer, L.A., 1990. Large-scale current-induced erosion and
613 deposition in the path of the 1929 Grand Banks turbidity current. Sedimentology 37, 613–629.
614 https://doi.org/10.1111/j.1365-3091.1990.tb00625.x

615 Inman, D.L., Nordstrom, C.E., Flick, R.E., 1976. Currents in Submarine Canyons: An Air-Sea-Land
616 Interaction. Annual Review of Fluid Mechanics 8, 275–310.
617 https://doi.org/10.1146/annurev.fl.08.010176.001423

618 Iverson, R.M., Logan, M., LaHusen, R.G., Berti, M., 2010. The perfect debris flow? Aggregated results
619 from 28 largescale experiments J. Geophys. Res., 115, Art. No. F03005.
620 https://doi.org/10.1029/2009JF001514

621 Khripounoff, A., Vangriesheim, A., Crassous, P., Etoubleau, J., 2009. High frequency of sediment gravity
622 flow events in the Var submarine canyon (Mediterranean Sea). Marine Geology 263, 1–6.
623 https://doi.org/10.1016/j.margeo.2009.03.014

624 Liu, J.T., Wang, Y.-H., Yang, R.J., Hsu, R.T., Kao, S.-J., Lin, H.-L., Kuo, F.H., 2012. Cyclone-induced
625 hyperpycnal turbidity currents in a submarine canyon. Journal of Geophysical Research: Oceans
626 117, C04033. https://doi.org/10.1029/2011JC007630

627 Lowe, D.R., 1976. Subaqueous liquefied and fluidised sediment flows and their deposits. Sedimentology,
628 23, 285–308. https://doi.org/10.1111/j.1365-3091.1976.tb00051.x

629 Maier, K.L., Gales, J.A., Paull, C.K., Rosenberger, K., Talling, P.J., Simmons, S.M., Gwiazda, R., McGann, M.,
630 Cartigny, M.J.B., Lundsten, E., Anderson, K., Clare, M.A., Xu, J., Parsons, D., Barry, J.P., Wolfson-
631 Schwehr, M., Nieminski, N.M., Sumner, E.J., 2019. Linking Direct Measurements of Turbidity
632 Currents to Submarine Canyon-Floor Deposits. Front. Earth Sci. 7, 144.
633 https://doi.org/10.3389/feart.2019.00144

634 Mangeney, A., Tsimring, L.S., Volfson, D., Aranson, I.S., Bouchut, F., 2007. Avalanche mobility induced by
635 the presence of an erodible bed and associated entrainment. Geophysical Research Letters 34,
636 L22401. https://doi.org/10.1029/2007GL031348

637 Nilsen, T.H., Shew, R.D., Steffens, G.S., Studlick, J.R.J. (Eds.), 2008. Atlas of Deep-Water Outcrops.
638 American Association of Petroleum Geologists, Oklahoma, U.S.A.
639 https://doi.org/10.1306/St561240

640 Pantin, H.M., 1979. Interaction between velocity and effective density in turbidity flow: Phase-plane
641 analysis, with criteria for autosuspension. Marine Geology 31, 59–99.
642 https://doi.org/10.1016/0025-3227(79)90057-4

643 Parker, G., 1982. Conditions for the ignition of catastrophically erosive turbidity currents. Marine
644 Geology 46, 307–327. https://doi.org/10.1016/0025-3227(82)90086-X

645 Parker, G., Fukushima, Y., Pantin, H.M., 1986. Self-accelerating turbidity currents. Journal of Fluid
646 Mechanics 171, 145. https://doi.org/10.1017/S0022112086001404

647 Paull, C.K., Caress, D.W., Lundsten, E., Gwiazda, R., Anderson, K., McGann, M., Conrad, J., Edwards, B.,
648 Sumner, E.J., 2013. Anatomy of the La Jolla Submarine Canyon system; offshore southern
649 California. Marine Geology 335, 16–34. https://doi.org/10.1016/j.margeo.2012.10.003

650 Paull, C.K., Caress, D.W., Ussler, W., Lundsten, E., Meiner-Johnson, M., 2011. High-resolution bathymetry
651 of the axial channels within Monterey and Soquel submarine canyons, offshore central
652 California. Geosphere 7, 1077–1101. https://doi.org/10.1130/GES00636.1

653 Paull, C.K., Mitts, P., Ussler III, W., Keaten, R., Greene, H.G., 2005. Trail of sand in upper Monterey
654 Canyon: offshore California. Geological Society of America Bulletin 117, 1134–1145.

655 Paull, C.K., Talling, P.J., Maier, K.L., Parsons, D., Xu, J., Caress, D.W., Gwiazda, R., Lundsten, E.M.,
656 Anderson, K., Barry, J.P., Chaffey, M., O'Reilly, T., Rosenberger, K.J., Gales, J.A., Kieft, B., McGann,
657 M., Simmons, S.M., McCann, M., Sumner, E.J., Clare, M.A., Cartigny, M.J., 2018. Powerful
658 turbidity currents driven by dense basal layers. Nature Communications 9, 4114.
659 https://doi.org/10.1038/s41467-018-06254-6

660 Paull, C.K., Ussler III, W., Caress, D.W., Lundsten, E., Covault, J.A., Maier, K.L., Xu, J., Augenstein, S., 2010.
661 Origins of large crescent-shaped bedforms within the axial channel of Monterey Canyon,
662 offshore California. Geosphere 6, 755–774. https://doi.org/10.1130/GES00527.1

663 Piper, D.J.W., Aksu, A.E., 1987. The source and origin of the 1929 grand banks turbidity current inferred
664 from sediment budgets. Geo-Marine Letters 7, 177–182. https://doi.org/10.1007/BF02242769

665 Piper, D.J.W., Cochonat, P., Morrison, M.L., 1999. The sequence of events around the epicentre of the
666 1929 Grand Banks earthquake: initiation of debris flows and turbidity current inferred from
667 sidescan sonar. Sedimentology 46, 79–97. https://doi.org/10.1046/j.1365-3091.1999.00204.x

668 Piper, D., Hundert, T., 2002. Provenance of distal Sohm Abyssal Plain sediments: history of supply from
669 the Wisconsinan glaciation in eastern Canada. Geo-Marine Letters 22, 75–85.
670 https://doi.org/10.1007/s00367-002-0101-2

671 Piper, D.J.W., Shor, A.N., Hughes Clarke, J.E., 1988. The 1929 “Grand Banks” earthquake, slump, and
672 turbidity current, in: Geological Society of America Special Papers. Geological Society of America,
673 pp. 77–92. https://doi.org/10.1130/SPE229-p77

674 Pouliquen, O., Forterre, Y., 2002. Friction law for dense granular flows: application to the motion of a
675 mass down a rough inclined plane. Journal of Fluid Mechanics 453, 133–151.
676 https://doi.org/10.1017/S0022112001006796

677 Salaheldin, T.M., Imran, J., Chaudhry, M.H., Reed, C., 2000. Role of fine-grained sediment in turbidity
678 current flow dynamics and resulting deposits. Marine Geology 171, 21–38.
679 https://doi.org/10.1016/S0025-3227(00)00114-6

680 Sequeiros, O.E., Mosquera, R., Pedocchi, F., 2018. Internal Structure of a Self-Accelerating Turbidity
681 Current. Journal of Geophysical Research: Oceans 123, 6260–6276.
682 https://doi.org/10.1029/2018JC014061

683 Sequeiros, O.E., Naruse, H., Endo, N., Garcia, M.H., Parker, G., 2009. Experimental study on self-
684 accelerating turbidity currents. Journal of Geophysical Research 114.
685 https://doi.org/10.1029/2008JC005149

686 Southard, J.B., Mackintosh, M.E., 1981. Experimental test of autosuspension. Earth Surface Processes
687 and Landforms 6, 103–111. https://doi.org/10.1002/esp.3290060204

688 Stevens, T., Paull, C.K., Ussler, W., McGann, M., Buylaert, J.-P., Lundsten, E., 2014. The timing of
689 sediment transport down Monterey Submarine Canyon, offshore California. Geological Society of
690 America Bulletin 126, 103–121. https://doi.org/10.1130/B30931.1

691 Stevenson, C.J., Feldens, P., Georgiopoulou, A., Schönke, M., Krastel, S., Piper, D.J.W., Lindhorst, K.,
692 Mosher, D., 2018. Reconstructing the sediment concentration of a giant submarine gravity flow.
693 Nat Commun 9, 2616. https://doi.org/10.1038/s41467-018-05042-6

694 Symons, W.O., Sumner, E.J., Talling, P.J., Cartigny, M.J.B., Clare, M.A., 2016. Large-scale sediment waves
695 and scours on the modern seafloor and their implications for the prevalence of supercritical
696 flows. Marine Geology 371, 130–148. https://doi.org/10.1016/j.margeo.2015.11.009

697 Talling, P.J., Paull, C.K., Piper, D.J.W., 2013. How are subaqueous sediment density flows triggered, what
698 is their internal structure and how does it evolve? Direct observations from monitoring of active
699 flows. Earth-Science Reviews 125, 244–287. https://doi.org/10.1016/j.earscirev.2013.07.005

700 Teledyne RD Instruments, 2011. Acoustic Doppler Current Profiler principles of operation: a practical
701 primer. P/N 951-6069-00. RD Instruments, San Diego, CA.

702 Traer, M.M., Hilley, G.E., Fildani, A., McHargue, T., 2012. The sensitivity of turbidity currents to mass and
703 momentum exchanges between these underflows and their surroundings. Journal of Geophysical
704 Research: Earth Surface 117, F01009. https://doi.org/10.1029/2011JF001990

705 Winterwerp, J.C., 2006. Stratification effects by fine suspended sediment at low, medium, and very high
706 concentrations. Journal of Geophysical Research 111. https://doi.org/10.1029/2005JC003019

Winterwerp, J.C., Bakker, W.T., Mastbergen, D.R., van Rossum, H., 1992. Hyperconcentrated Sand-Water Mixture Flows over Erodible Bed. Journal of Hydraulic Engineering 118, 1508–1525. https://doi.org/10.1061/(ASCE)0733-9429(1992)118:11(1508)

Winterwerp, J.C., de Groot, M.B., Mastbergen, D.R., Verwoert, H., 1990. Hyperconcentrated Sand-Water Mixture Flows Over a Flat Bed. Journal of Hydraulic Engineering 116, 36–54. https://doi.org/10.1061/(ASCE)0733-9429(1990)116:1(36)

Xu, J.P., 2010. Normalized velocity profiles of field-measured turbidity currents. Geology 38, 563–566. https://doi.org/10.1130/G30582.1

Figures

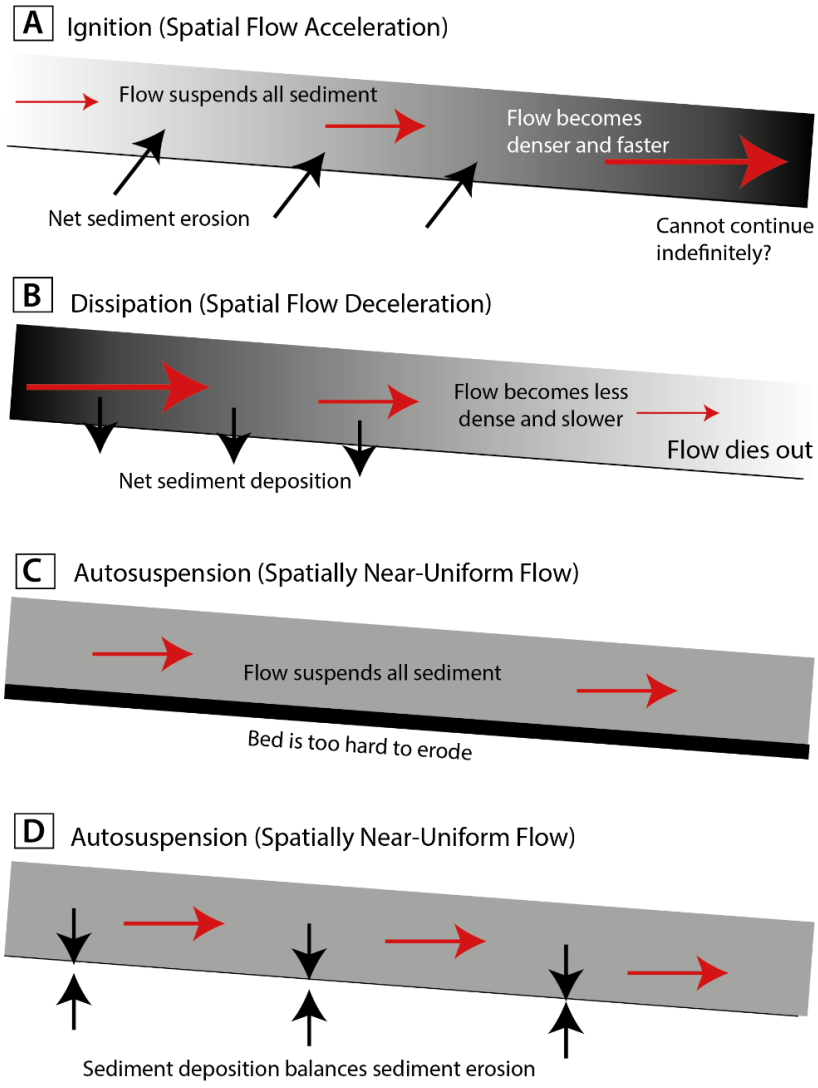

Figure 1. Ignition, dissipation and autosuspension of turbidity currents. **(A)** Ignition is caused by net sediment erosion that increases flow density, causing increased velocities. This positive feedback cannot continue indefinitely, as elevated sediment concentrations eventually damp turbulence, shield the bed from erosion, or increase friction. **(B)** Dissipation is caused by sediment deposition, which leads to spatial decreases in flow density, and thus velocity. This negative feedback causes the flow to eventually die out. **(C and D)** Autosuspension comprises a situation in which flow density remains constant, and flow velocities are constant spatially. **(C)** Flow may be powerful enough to suspend all of the sediment it carries, but the substrate is too hard to erode. Alternatively, localised areas of erosion and deposition may also balance each other out, leading to no net change in suspended sediment. (**D)** Sediment deposition may be balanced by an equal amount of substrate erosion. Models for autosuspension in (C) and (D) assume flow is dilute and fully turbulent. We subsequently present an alternative model for autosuspension (Fig. 7), where flow is driven by a dense near-bed layer.

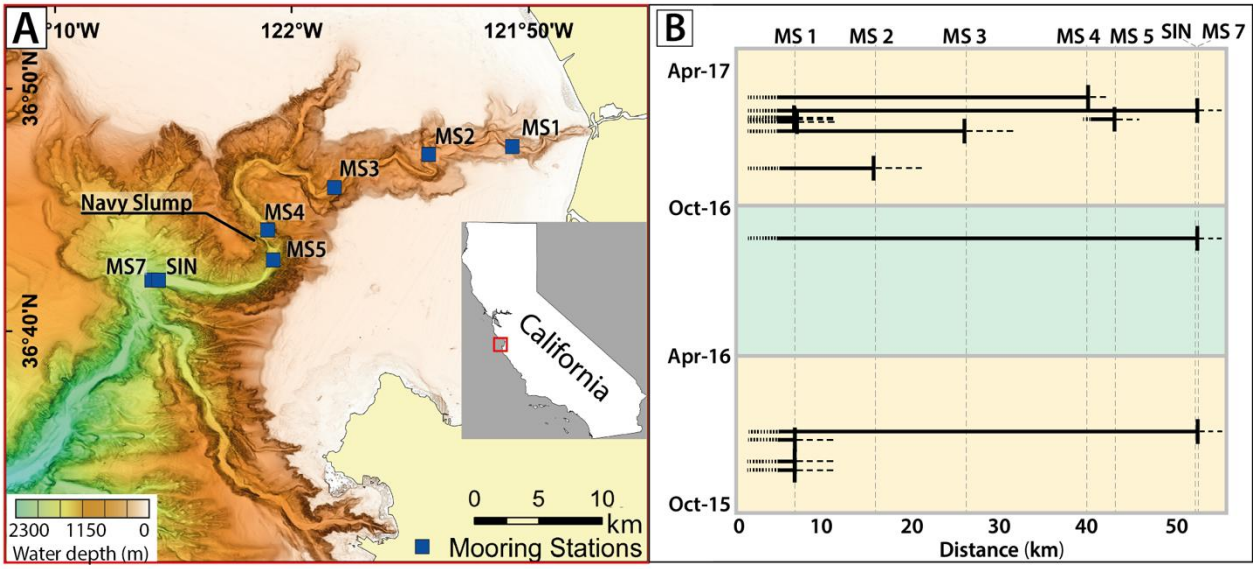

733
734

735 **Fig. 2. Location, runout distances and velocities of turbidity currents in Monterey Canyon.**
736 **(A)** Bathymetry map of Monterey Canyon showing location of moorings in this study (MS1 to
737 MS7, SIN), and Navy Slump. **(B)** Timing and runout distance of turbidity currents in Monterey
738 Canyon between October 2015 and April 2017. Horizontal lines show 13 events registered by
739 ADCPs. The green and yellow boxes show the 6-month deployment periods. Locations of
740 moorings (MS1 to MS7, SIN) are indicated. The exact point where flows terminate between
741 moorings is uncertain. **(C)** Changes in flow velocity with distance along Monterey Canyon's
742 thalweg. Solid dots and solid lines show frontal velocities between moorings. Open symbols and
743 dotted lines show maximum internal velocity measured at each mooring by an ADCP, including
744 for some flows that only reached the first mooring (solid squares). **(D)** Changes in thalweg
745 gradient. **(E)** Changes in axial channel width, defined by the width of mapped bedforms.
746

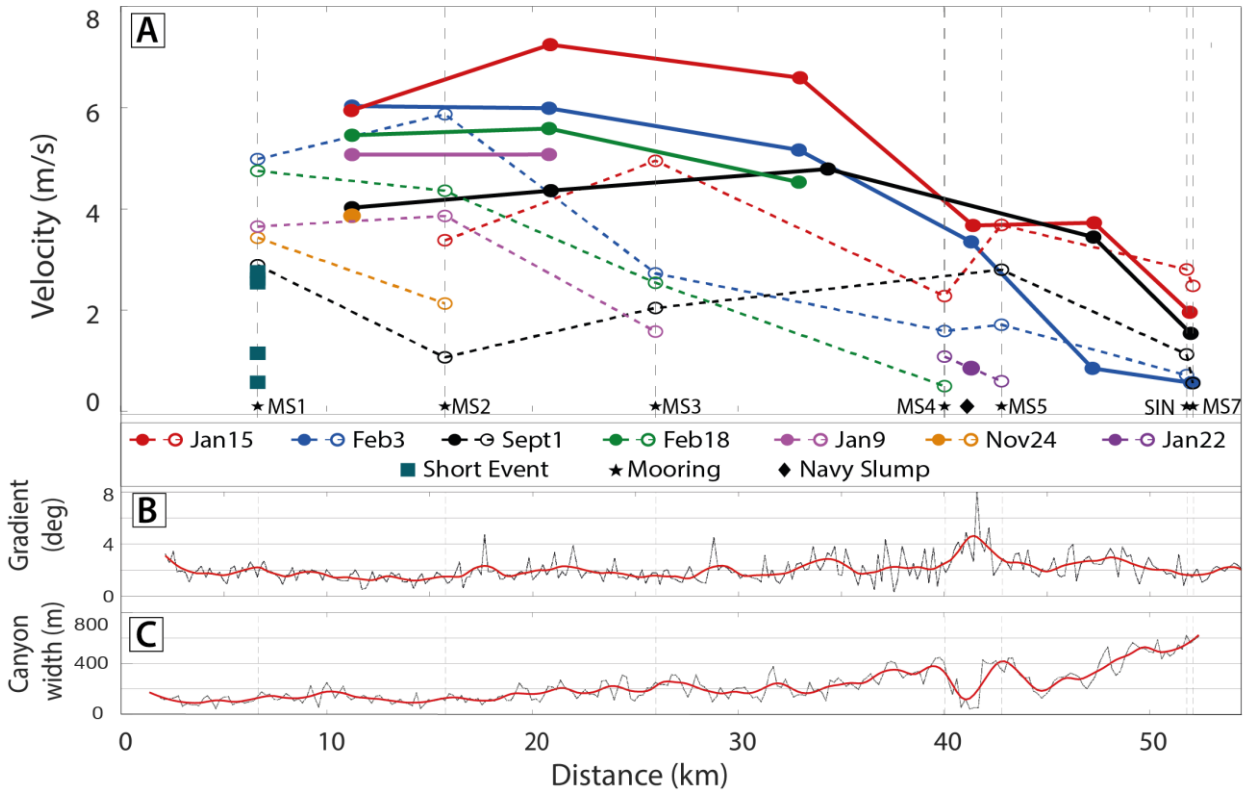

Fig. 3. Velocities of turbidity currents in Monterey Canyon and properties of the thalweg. **(A)** Changes in flow velocity with distance along Monterey Canyon's thalweg. Solid dots and solid lines show frontal velocities between moorings. Open symbols and dotted lines show maximum internal velocity measured at each mooring by an ADCP, including for some flows that only reached the first mooring (solid squares). **(B)** Changes in thalweg gradient. **(C)** Changes in axial channel width, defined by the width of mapped bedforms.

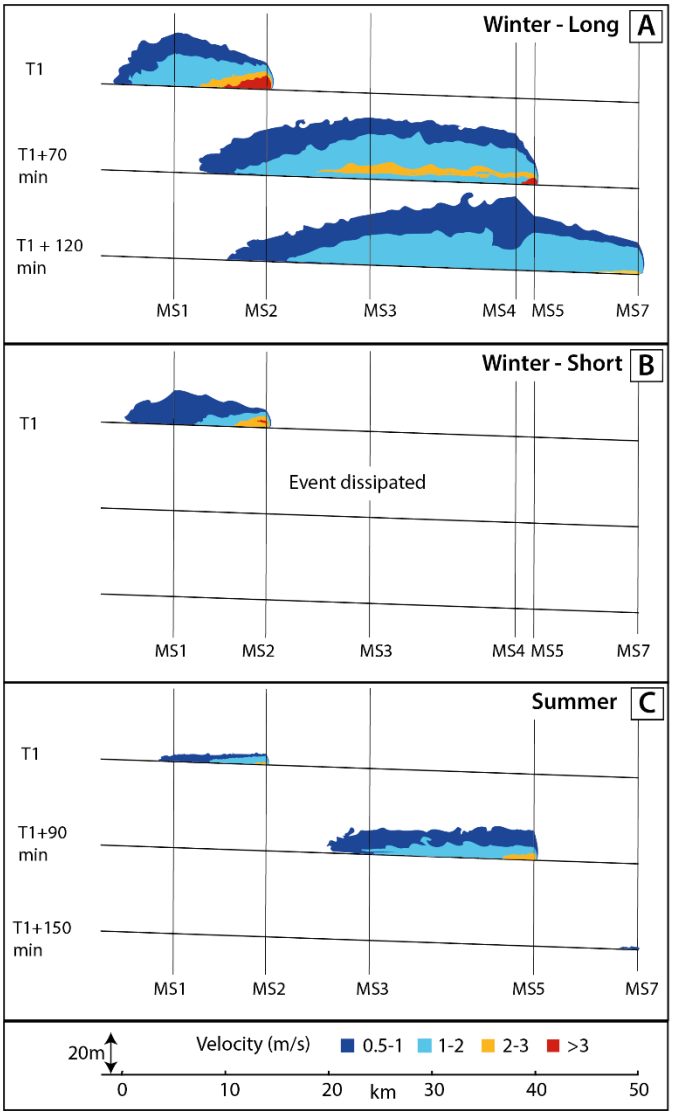

Fig. 4. Turbidity current structure at consecutive snap-shots in time, showing changes in flow-length, internal velocity-structure, and flow-thickness. Flow velocities between moorings are inferred, as are velocities in the lower 3-4 m of the flow (due to ADCP side-lobe interference). **(A)** Long run-out flow, which is initially fast, based primarily on the January 15th event. The MS1 mooring was dragged down-canyon during the January 15th event. Thus, ADCP-data from the February 3rd event are used for MS1 in T1 snapshot, and it is unknown if the 15th January flow was present at MS1 during the T1+70 min snapshot. **(B)** Shorter runout flow that was initially powerful, but then dissipated rapidly, based on November 24th event. This event carried an 800 kg object at ≥ 4 m/s, for ~1 km in the upper canyon (Paull et al., 2018). **(C)** Example of an initially-weak turbidity current on September 1st, which then accelerated markedly in the mid-canyon, and dissipated rapidly between MS5 and MS7. This is the only event that occured during summer months (Fig. 2b).

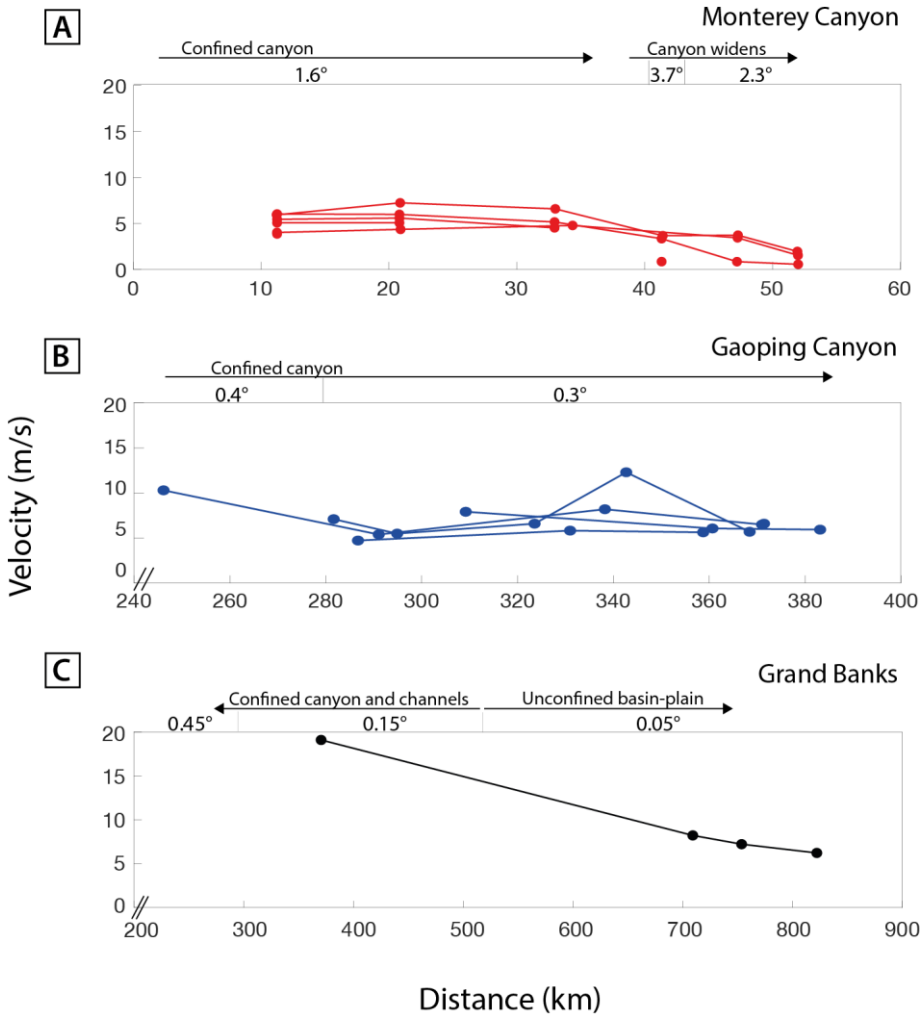

Fig. 5. Changes in frontal velocities of turbidity currents over distance. Variations in seabed gradient and flow confinement are also shown. **(A)** Frontal velocities of flows in Monterey Canyon. Figure 3 shows detailed changes in seabed gradient and channel floor width. **(B)** Frontal velocities of flows confined within Gaoping Canyon, offshore Taiwan, based on cable breaks (Gavey et al. 2017*)*. Average seabed gradients are shown, but detailed surveys of canyon width are currently lacking. **(C)** Frontal velocities of the Grand Banks turbidity current in 1929, offshore Newfoundland, based on cable breaks (Heezen and Ewing, 1952; Hughes Clarke, 1988; Piper et al., 1999). Distance is from the initial earthquake epicentre, although coincident cable breaks occurred over a wider area. The initial part of this flow was confined by submarine fan-valleys, but was unconfined during its later stages, as it spread across a basin plain (Piper et al., 1999). Detailed data on the seafloor gradient over the entire length of the event are lacking, and are based on Stevenson et al. (2018) and Piper and Hundert (2002).

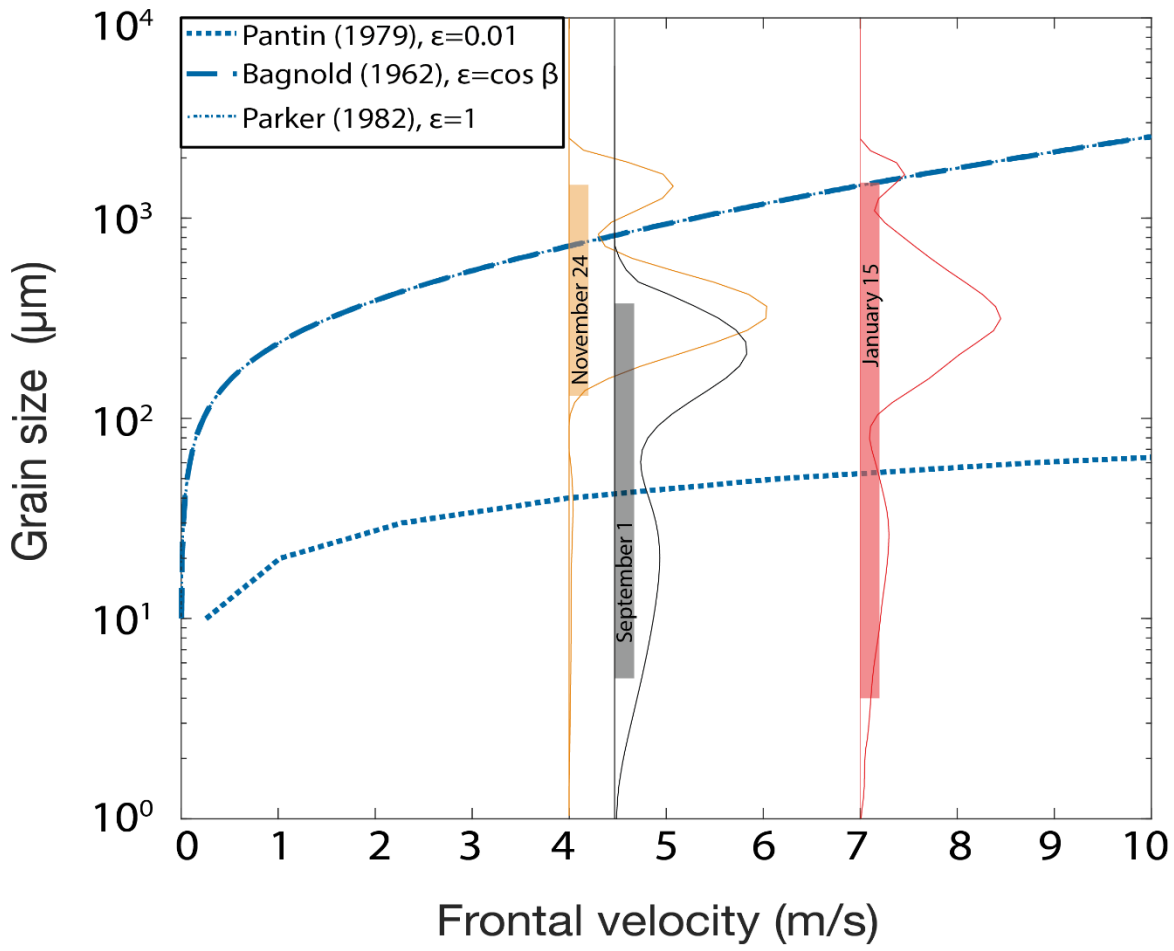

Fig. 6. Comparison of field measurements in Monterey Canyon to past energy-balance theory for autosuspension, following Sequeiros et al. (2009). It shows the threshold flow velocity predicted by three past theories, for a given grain-size and seabed gradient, above which flows carry all suspended sediment (i.e. autosuspend). If seabed sediment is available for erosion, the flow will also ignite. Blue lines show the different threshold constants (ε in Equation 1) used by different authors, assuming a seabed gradient of 2°. Autosuspension occurs below the lines. Note that results for the threshold constant of Bagnold (1962) coincide with those of Parker (1982) for the case of Monterey Canyon. Grain-size distributions for three events (November 24th, September, 1st, and January 15th) in Monterey Canyon, based on sediment traps located 10 m above the bed. The grain-size distributions shown here are averages for each event in sediment traps from the upper canyon where flows are assumed to ignite (see Material and Methodology, Supplementary Fig. 5 for more information). The coloured boxes show the 10th percentile (D_{10}) and 90th percentile (D_{90}) of the coarsest grain-size samples in traps from each event.

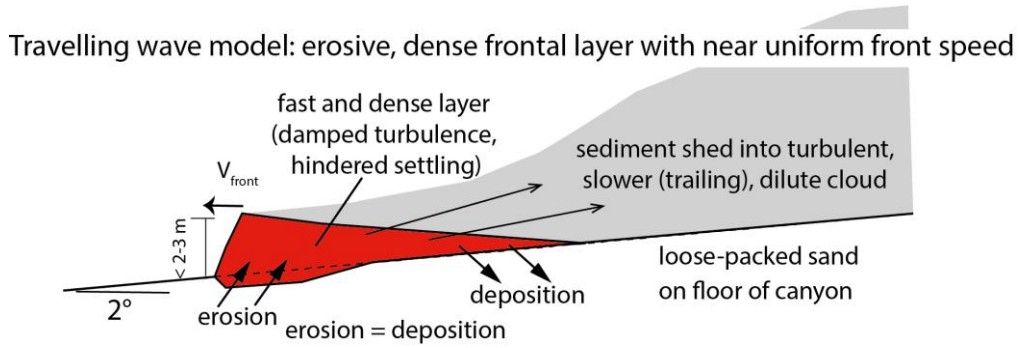

Fig. 7. New travelling wave model. Travelling wave model for turbidity current behaviour in loose-sand submarine canyons, in which flows contain a fast and dense near-bed layer at their front, as proposed by (Paull et al., 2018). Erosion at the front of this dense near-bed layer is balanced by sediment deposition from its rear, leading to uniform transit velocity and autosuspension. Sediment is shed backwards to form a trailing sediment cloud that is dilute and fully turbulent, which lengthens over time.

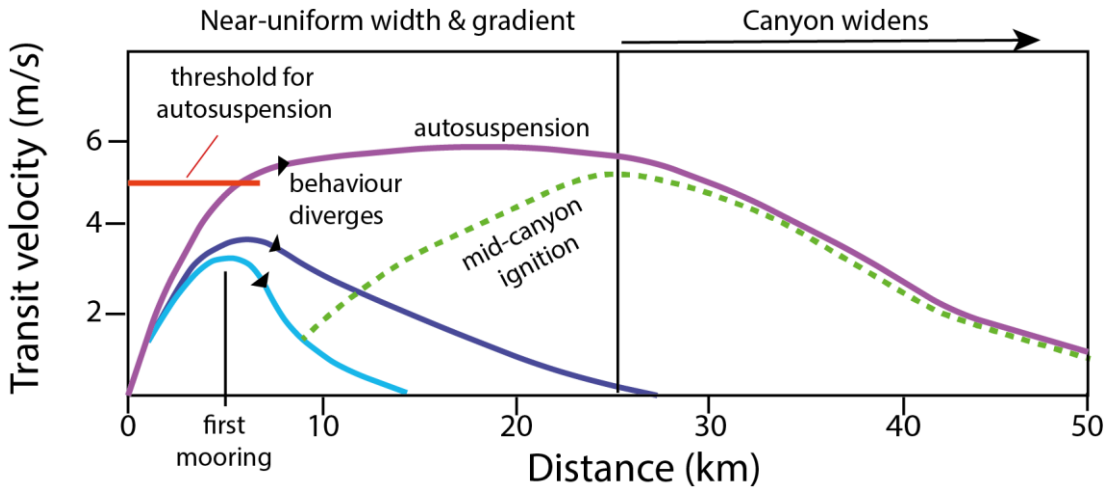

Fig 8. Summarising model for turbidity current behaviour in submarine canyons underlain by loose sand. Patterns of flow behaviour, based on frontal transit velocities that are simplified from Fig. 3a. Small increases in transit velocity at the first mooring are associated with major differences in subsequent flow velocities and runout distance, causing divergence in flow behaviour (purple, dark blue and light blue lines). However, flows can sometimes self-accelerate and ignite within the mid-canyon (green dotted line), due to changes in substrate strength and erodibility. There is a threshold initial transit velocity (red line) above which flows can autosuspend (purple line).

Table 1

Flow Threshold	≥1 m/s							≥2 m/s							≥3 m/s						
Mooring	MS 1	MS 2	MS 3	MS 4	MS 5	SIN	MS 7	MS 1	MS 2	MS 3	MS 4	MS 5	SIN	MS 7	MS 1	MS 2	MS 3	MS 4	MS 5	SIN	MS 7
Distance (km)	6.7	16	26.0	40.0	43	51.8	52	6.7	16	26.0	40.0	43	51.8	52	6.7	16	26.0	###	43	###	52
Jan-15		87	141	182	213	112	89		9.5	59	23	41	37	22		8.5	30	0	25	0.5	0
Sep-01	20	3.5	73		22	45	0	1	0.5	7	0	11	0	0	0.5	0	0	0	3	0	0
Feb-03	48	74	73	67	65	0	0	28	17	26	0	3.5	0	0	16	15	2.5	0	0	0	0
Feb-18	34	26	70	0				15	12	16					7.5	8	1.5				
Jan-09	35	23	43					19	11	0					11	8	0				
Nov-24	33	15						12	3.5						9	0.5					
Jan-21	31							9.5							2						
Jan-20	25							7							2.5						
Dec-01	16							7							3						
Jan-23	9							0							0						
Jan-06	6.5							1							0						
Dec-11	2.5							0							0						
Jan-22				37	0						0	0						0	0		

Table 1. Flow duration (in minutes) for each mooring station and event. For each event, a threshold flow velocity was set to determine the duration of the flow at each mooring. The ADCP data was displayed using contour lines corresponding to each threshold, allowing for determination of flow duration at every mooring. Left hand columns denote flow velocity threshold ≥ 1 m/s. Middle columns denote flow

velocity threshold ≥ 2 m/s. The right-hand column denotes flow velocity threshold ≥ 3 m/s. Where no flow duration is given, there was no ADCP measurement (January 15, MS1, and September 1, MS4). A duration of 0 min indicates the flow is no longer measured at the specified threshold velocity at that mooring.

Graphical Abstract:

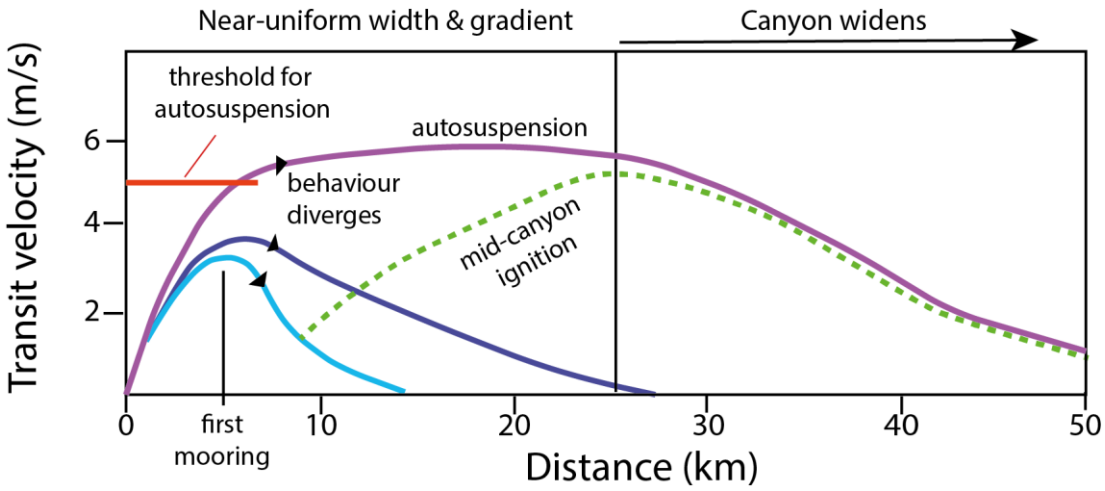

Summarising model for turbidity current behaviour in submarine canyons underlain by loose sand. Small increases in initial velocity cause major differences in subsequent flow velocities and runout distance, causing divergence in flow behaviour (purple, dark blue and light blue lines). However, flows can sometimes self-accelerate and ignite within the mid-canyon (green dotted line), due to changes in substrate strength and erodibility. There is a threshold initial transit velocity (red line) above which turbidity currents can autosuspend (purple line).